A series of nano/micro-sized metal-organic frameworks with tunable photoluminescence properties

Zheng, Yuhua; Liu, Kai; Sun, Xun; Guan, Rengui; Su, Huijuan; You, Hongpeng; Qi, Caixia

Published in:
CrystEngComm

DOI:
10.1039/c4ce02456g

Publication date:
2015

CrystEngComm

PAPER

View Article Online
View Journal | View Issue

Cite this: *CrystEngComm*, 2015, **17**, 2321

A series of nano/micro-sized metal–organic frameworks with tunable photoluminescence properties†

Yuhua Zheng,[a] Kai Liu,[b] Xun Sun,[a] Rengui Guan,[a] Huijuan Su,[a] Hongpeng You*[c] and Caixia Qi*[a]

Received 12th December 2014,
Accepted 2nd February 2015

DOI: 10.1039/c4ce02456g

www.rsc.org/crystengcomm

Present studies on metal–organic frameworks (MOF) mainly focus on macro-scaled single crystals. However, the realization of MOF nanocrystals *via* a bottom-up one-step method still remains a significant challenge. Here, hierarchically assembled nanostructures of lanthanide-based MOFs with 1D and 3D morphologies have been successfully fabricated *via* a simple and rapid solution phase method at room temperature. Upon UV excitation, these nanomaterials exhibit highly efficient tunable luminescence properties, which come from the Eu^{3+} or Tb^{3+} ions. Moreover, white-light emission can be achieved by co-activating the organic ligand, Eu^{3+} and Tb^{3+} ions in the nano-MOFs.

1. Introduction

Metal–organic frameworks (MOFs), in which metal ions or metal clusters are connected by molecular building blocks consisting of organic molecules or organometallic complexes, have attracted a great deal of attention[1–4] due to their well-defined coordination geometries and useful applications in gas storage, catalysis, optics, recognition, and separation. In the past two decades, a structural study of macro-scaled crystalline samples is of main fundamental interest in metal–organic materials based on single-crystal X-ray analysis. However, miniaturization of the size of MOF crystals to the nanometer scale by functionalizing the crystal interfaces will provide further opportunities to integrate novel functions into the materials without changing the characteristic features of the metal–organic crystal itself, and will allow the correlation between the chemical and physical properties and interfacial structures of nanocrystalline MOFs (nano-MOF) to be investigated. Recently, several nano- and micro-scaled particles from metal–organic complexes have been successfully prepared by solvent-induced precipitation,[5] reverse microemulsion,[6] electrospinning,[7] hydrothermal,[8] and solvothermal methods.[9] These thought-provoking studies suggest that the suitable design of reaction routes and selection of the metal ions and ligands could open a new field for preparing nano/micro-scaled metal–organic materials from the molecular level, enabling their use in a broad range of applications[10–15] including catalysis, biosensing, biomedical imaging, and anticancer drug delivery. However, the introduction of high temperature or pressure for the fabrication of nanoarchitectures induces heterogeneous impurities, increases the production cost, and leads to difficulties in scale-up production.

Lanthanide-based MOFs have been extensively investigated, acting as luminescent devices, magnets, catalysts, and other functional materials, because of their electronic, optical, and chemical characteristics resulting from the 4f electronic shells.[16–21] In our previous work, some nano-sized metal–organic compounds based on lanthanide ions (Ln^{3+}) and benzenetricarboxylic acid (BTC) have been constructed successfully.[22–25] For example, 1D nanobelts based on the coordinated assembly of Tb^{3+} ions and BTC ligands have been fabricated.[25] The luminescent color of the nanobelts can be easily shifted from green to green-yellow, yellow, orange and red-orange by doping with Eu^{3+} ions (Tb–BTC: Eu^{3+}). However, it is still a challenge to develop a general strategy regarding the rational choice of different lanthanide ions for tuning nano-MOF assemblies. Moreover, the selection of suitable host-activators and precise control of different combinations of doped Ln^{3+} ions are consistently needed for highly efficient tunable nano-MOF luminescence. Herein, we present the successful preparation of a series of nano-MOFs (Y–BTC, Gd–BTC, Ce–BTC, Sm–BTC, and Tm–BTC) with 1D and 3D architectures on a large scale *via* one-step precipitation in the solution phase under ambient conditions

[a] *Shandong Applied Research Center for Gold Nanotechnology (Au-SDARC), School of Chemistry and Chemical Engineering, Yantai University, Yantai 264005, PR China. E-mail: qicx@ytu.edu.cn*
[b] *Department of Polymer Chemistry, Zernike Institute for Advanced Materials, University of Groningen, Nijenborgh 4, 9747 AG Groningen, The Netherlands*
[c] *State Key Laboratory of Rare Earth Resource Utilization, Changchun Institute of Applied Chemistry, Chinese Academy of Sciences, Changchun 130022, PR China. E-mail: hpyou@ciac.ac.cn*

† Electronic supplementary information (ESI) available. See DOI: 10.1039/c4ce02456g

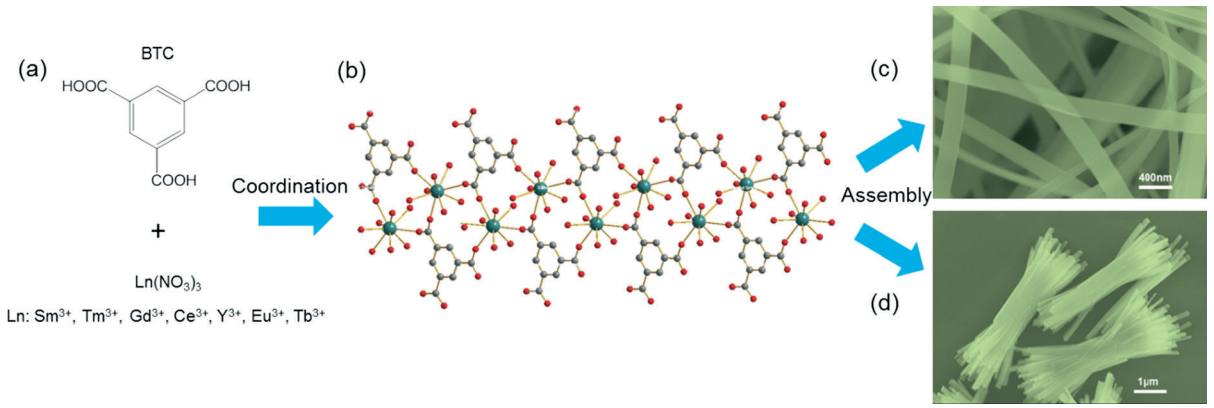

Fig. 1 Schematic route for the preparation of nano/micro-sized crystals of lanthanide benzenetricarboxylate (Ln–BTC). (a) The used building blocks: a series of lanthanide nitrates and organic ligand 1,3,5-benzenetricarboxylic acid. (b) The formed 1D ribbon-like molecular motifs of Ln–BTC (the hydrogen atoms were omitted for clarity, Ln = dark green, O = red, C = gray). (c, d) Coordination induced assembly of Ln–BTC nanocrystals with 1D and 3D architectures.

(Fig. 1). Emission colors are tunable in these nano-MOFs by doping with Eu^{3+} and Tb^{3+} ions. Very interestingly, white light emission can be achieved by the combination of photoluminescence characteristics of the BTC ligand and Eu^{3+} and Tb^{3+} ions codoped in the Ce–BTC host.

2. Experimental parts

2.1 Materials

The rare earth oxides, including Y_2O_3, Gd_2O_3, Sm_2O_3, Tm_2O_3, Eu_2O_3 and Tb_4O_7 (99.99%), were purchased from Wuxi Yiteng Rare-Earth Limited Corporation (China). 1,3,5-Benzenetricarboxylic acid (BTC) (98%) was purchased from Alfa Aesar Chemical Company. HNO_3 and ethanol (both with purity of A. R.) were purchased from Beijing Fine Chemical Company (China). All of the chemicals were used directly without further purification.

2.2 Preparation

$Ln(NO_3)_3$ aqueous solution (pH = 3–4) was obtained by dissolving Y_2O_3, Gd_2O_3, Sm_2O_3, Tm_2O_3, Eu_2O_3 and Tb_4O_7 in dilute HNO_3 solution under heating with agitation. In a typical synthesis of Tm–BTC/Sm–BTC nanocrystals, 4 mL of 0.5 M $Tm(NO_3)_3$ or $Sm(NO_3)_3$ aqueous solution was added into 40 mL of 0.05 M BTC ethanol–water solution (v/v = 1 : 1) under vigorous stirring at room temperature, and a large amount of white precipitate was formed. After reaction for 30 min, the precipitate was collected by centrifugation, washed several times with ethanol and water, and dried in air for characterization. A similar process was employed to prepare $Gd_{0.95}Eu_{0.05}$–BTC, $Gd_{0.95}Tb_{0.05}$–BTC, $Ce_{0.90}Eu_{0.05}Tb_{0.05}$–BTC, and $Y_{0.95}Eu_{0.05}$–BTC, except for adding the mixed $Ln(NO_3)_3$ aqueous solutions (*e.g.*, 4 mL of 0.5 M $Gd(NO_3)_3$ + 0.21 mL of 0.5 M $Eu(NO_3)_3$) at the initial stage, while other reaction parameters were kept unchanged.

2.3 Characterization

Powder X-ray diffraction (XRD) patterns were obtained using a D8 Focus (Bruker) diffractometer (continuous, 40 kV, 40 mA, increment = 0.02°). Thermogravimetric analysis (TGA) data were recorded with a thermal analysis instrument (SDT 2960, TA Instruments, New Castle, DE) at a heating rate of 10 °C min^{-1} in an air flow of 100 mL min^{-1}. The morphology and composition of the samples were inspected using a field emission scanning electron microscope (FE-SEM, S-4800, Hitachi) equipped with an energy dispersive X-ray spectroscope (EDX, JEOL JXA-840). Photoluminescence excitation and emission spectra were recorded with a Hitachi F-4500 spectrophotometer equipped with a 150 W xenon lamp as the excitation source.

3. Results and discussion

Nano-MOFs of Ln–BTC (Sm–BTC, Tm–BTC, $Gd_{0.95}Eu_{0.05}$–BTC, $Gd_{0.95}Tb_{0.05}$–BTC, $Ce_{0.90}Eu_{0.05}Tb_{0.05}$–BTC, and $Y_{0.95}Eu_{0.05}$–BTC) were prepared by directly mixing $Ln(NO_3)_3$ and BTC solutions (Fig. 1a). Due to the strong coordinated interactions between the Ln^{3+} ions and carboxylic acids of BTC, the formed hydrophobic Ln–BTC was precipitated efficiently from an aqueous environment. After centrifugation and dehydration, the purified Ln–BTC samples were first analyzed by powder X-ray diffraction (XRD). As shown in Fig. 2, all the samples were well-crystallized in spite of the moderate reaction conditions. All of the diffraction peaks can be well indexed to the bulk phase of La–BTC.[26] Their structure can thus be monoclinic with the space group *Cc*. No peaks of impurities were detected, indicating that all the Ln^{3+} ions have been effectively coordinated with the BTC ligand. The center Ln atom is nine-coordinated by three oxygen atoms from three carboxylate groups of BTC ligands as well as six oxygen atoms from water molecules to form a tricapped trigonal prismatic geometry (Fig. S1†). As shown in Fig. 1b, the Ln–BTC MOF structure consists of parallel ribbon-like molecular

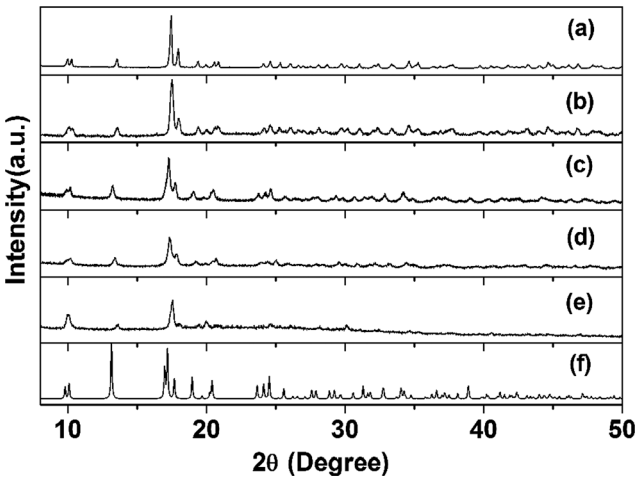

Fig. 2 XRD patterns of the as-prepared Ln–BTC nanocrystals (a, $Y_{0.95}Eu_{0.05}$–BTC 1D nanobelts; b, $Gd_{0.95}Eu_{0.05}$–BTC 1D nanorods; c, $Ce_{0.90}Eu_{0.05}Tb_{0.05}$–BTC 3D nanobundles; d, Sm–BTC 3D nanobundles; e, Tm–BTC 3D nanobundles) and simulated XRD pattern using the X-ray structure of La(BTC) single crystal (f).[26] These results reveal that the obtained samples are isostructural with the La–BTC structure. The spectral shift of the diffraction peaks can be explained by the change in ionic radii.

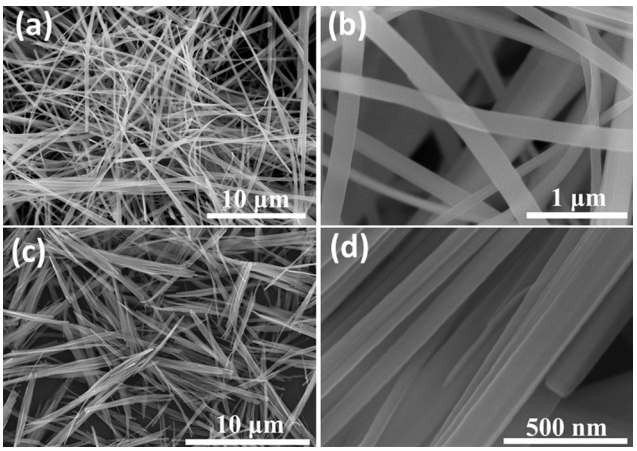

Fig. 3 SEM images of the Ln–BTC 1D nanocrystals. (a, b) The obtained $Y_{0.95}Eu_{0.05}$–BTC nanobelts. (c, d) The obtained $Gd_{0.95}Eu_{0.05}$–BTC nanorod bundles. The growth of 1D nanocrystals is largely determined by the anisotropic nature of the Ln–BTC structure.

motifs extending along one direction, which could be the reason for the 1D nanobelt formation (Fig. 1c). In addition, the combination of noncovalent interactions (hydrogen bonding and π–π stacking of phenyl groups) could lead to the formation of a 3D network structure (Fig. S1†), which may be useful for the micro-scaled assembly in 3D directions (Fig. 1d). In addition, a spectral shift of the diffraction peaks has been detected (Fig. 2), which can be explained by the change in ionic radii. For example, when the La^{3+} ions were substituted by the Tm^{3+} ions with a smaller radius as a result of lanthanide contraction, the crystal lattice constants as well as the *d*-spacing decreased, and thus the diffraction angles increased accordingly because of the Bragg equation, $\sin\theta = \lambda/2d$, where d is the distance between two crystal planes, θ is the diffraction angle of an observed peak, and λ is the X-ray wavelength (1.54 Å). Furthermore, the thermal behaviors of these samples were investigated by thermal gravimetric analysis (TGA). These TGA curves (Fig. S1†) exhibited two major stages of rapid weight loss in the temperature range from 80 to 1000 °C. The weight loss for the two stages was measured to be ~25 and ~45%, respectively, which is basically in agreement with the theoretical weight loss of the six water molecules (23.68%) and the organic ligand (38.96%) of the assumed structure $Ln(BTC)(H_2O)_6$. This indicated that six water molecules are coordinated in the MOF structure, matching well the structure analysis of bulky La(BTC).[26]

The morphology of the prepared nano-MOF was characterized by scanning electron microscopy (SEM). The low-magnification SEM images (Fig. 3a) revealed that $Y_{0.95}Eu_{0.05}$–BTC consists of a large quantity of well-dispersed 1D nanostructures with lengths of 20–50 μm. The obvious creasing or curling places in the higher magnification SEM image (Fig. 3b) provided evidence that the as-synthesized products possess a belt-like shape. It can be clearly seen that these nanobelts exhibit smooth surfaces, which are about 100–200 nm in width. The energy-dispersive X-ray spectra (EDX) of the nanobelts show several peaks corresponding to Y, Eu, C, and O elements in the range of 0–10 keV (Fig. S3a†), indicating that these nanobelts are formed from yttrium, europium, and benzenetricarboxylate, and the molar ratios of the metal ions matched well with the assumed compound formula. Fig. 3c and d show the $Gd_{0.95}Eu_{0.05}$–BTC products obtained under the same conditions. Instead of nanobelt formation, nanobundles appeared which are composed of several nanorods. The 1D nanorods exhibited a smooth surface and rectangular cross section, without any creasing or curling places. They have widths of about 150–200 nm, thicknesses of ~50 nm, and lengths of around several micrometers. Fig. S2b† shows the EDS spectrum of the final product, confirming that no elements other than C, O, Gd, and Eu are present except for the Si and Pt peaks from the measurement. It is well-known that preferential growth often occurs in a crystal with structural anisotropy which has a relatively small lateral adhesion energy.[27] In the present experiments, the formation of $Y_{0.95}Eu_{0.05}$–BTC nanobelts and $Gd_{0.95}Eu_{0.05}$–BTC nanorod bundles is largely determined by the anisotropic nature of the MOF structure. As shown in Fig. 1b, one can see that the interesting feature of the compound is the presence of a 1D ribbon-like molecular motif formed by the coordinating interactions between the Ln^{3+} ion and the BTC ligand. Thus, it suggests that the formed 1D ribbon-like structure could be responsible for the anisotropic nucleation and growth process of the 1D Ln–BTC nanostructures.

When BTC was reacted with other lanthanide ions (Sm^{3+}, Tm^{3+}, and Ce^{3+}), the morphology of these Ln(BTC) products changed to 3D nanoarchitectures assembled by 1D nanobelt or nanorod units. Fig. 4a and b show typical SEM images of the uniform and well-dispersed straw-sheaf-like $Ce_{0.90}Eu_{0.05}Tb_{0.05}$–BTC assemblies on a large scale. The

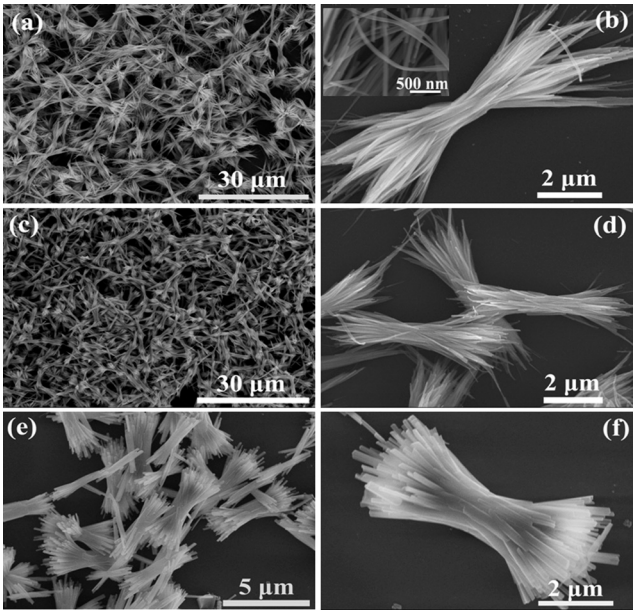

Fig. 4 SEM images of the Ln–BTC 3D nanocrystalline architectures. (a, b) The obtained $Ce_{0.90}Eu_{0.05}Tb_{0.05}$–BTC 3D straw-sheaf structures. (c, d) The obtained Sm–BTC 3D straw-sheaf structures. Both of them are assembled by outspread and flexible nanobelts. (e, f) The obtained Tm–BTC 3D straw-sheaf architectures, where the straw-sheaves are composed of rigid nanorods.

product looks like a straw-sheaf with two fantails consisting of a bundle of outspread and flexible nanobelts, which are closely bonded to each other in the middle, so it is called a "straw-sheaf structure". Careful observations revealed that an individual straw-sheaf has a length in the range of 7–10 μm and a middle diameter in the range of 1–1.5 μm. The prepared Sm–BTC also gave similar straw-sheaf-like microstructures, as confirmed by Fig. 4c and d. More interestingly, when the Tm^{3+} ions were mixed with BTC, the generated nano-MOF architectures were entirely composed of straw-sheaves with more obvious radiating fantails, as shown in Fig. 4e and f. These morphological characteristics demonstrate that a sheaf of rigid rod-like crystals has been bandaged in the middle, with the top and bottom fanning out while the middle remaining thin. The formation process of hierarchical architectures is a complex process, which is affected by both crystal growth environments and crystal structures, including the degree of supersaturation, diffusion of the reaction species, surface energy, and so forth.[28] The formation of these present hierarchical architectures is considered to be a crystal splitting process, as evidenced by some inorganic nanomaterials[29,30] and our previous results.[23,24]

The photoluminescence properties of Ln–BTC assemblies were investigated in detail. Fig. 5a shows the excitation and emission spectra of the $Gd_{0.95}Eu_{0.05}$–BTC nanorods. The broadband excitation with two maxima at 260 and 292 nm is due to the charge-transfer band between the O^{2-} and Eu^{3+} ions and the π–π* electron transition of the organic bridging ligand, respectively.[22,31] Under excitation at 268 nm, the emission spectrum consists of two main peaks at about 589

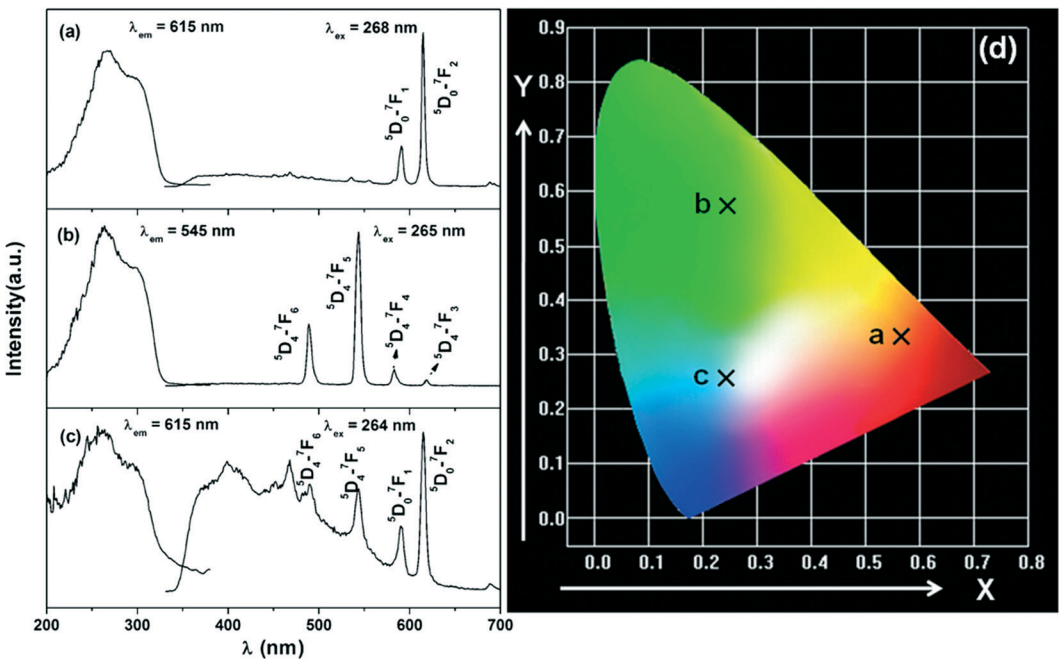

Fig. 5 Photoluminescence properties of the as-prepared Ln–BTC nanocrystals. (a) Excitation and emission spectra of the $Gd_{0.95}Eu_{0.05}$–BTC nanorods, showing characteristic emission of the Eu^{3+} ions. (b) Excitation and emission spectra of the $Gd_{0.95}Tb_{0.05}$–BTC nanorods, showing characteristic emission of the Tb^{3+} ions. (c) Excitation and emission spectra of the $Ce_{0.90}Eu_{0.05}Tb_{0.05}$–BTC nanoarchitectures. The co-existing blue, green, and red emission approach the white-light region, indicating the partial energy transfer from the BTC ligand to the Eu^{3+} and Tb^{3+} ions. (d) CIE chromaticity diagram of $Gd_{0.95}Eu_{0.05}$–BTC (a point 0.565, 0.334), $Gd_{0.95}Tb_{0.05}$–BTC (b point 0.245, 0.572), and $Ce_{0.90}Eu_{0.05}Tb_{0.05}$–BTC (c point 0.243, 0.256), confirming the tunable photoluminescence by doping or codoping with Eu^{3+} and Tb^{3+} ions.

and 615 nm, which are assigned to the $^5D_0$–$^7F_1$ and $^5D_0$–$^7F_2$ transitions of the Eu^{3+} ions, respectively. This result indicates that the Eu^{3+} ions are essentially excited by host Gd–BTC absorption. When the Tb^{3+} ions were doped into the same host, the excitation was similar while the emission exhibited four peaks centered at 489, 544, 585, and 620 nm, which correspond to the $^5D_4$–^7F_J (J = 6, 5, 4 and 3) transitions of the Tb^{3+} ions, respectively (Fig. 5b). Furthermore, the $Y_{0.95}Eu_{0.05}$–BTC nanobelts exhibited characteristic emission of the Eu^{3+} ions (Fig. S3†). These results indicated the efficient energy transfer from the nano-MOF Ln–BTC host to the doped Eu^{3+} and Tb^{3+} ions. However, the emission spectra of the $Ce_{0.90}Eu_{0.05}Tb_{0.05}$–BTC sample excited at 264 nm exhibited not only the characteristic emission of the Eu^{3+} and Tb^{3+} ions, but also the blue emission of the BTC ligand (Fig. 5c). The stronger broadband in the range from 350 to 550 nm comes from the emission of BTC in $Ce_{0.90}Eu_{0.05}Tb_{0.05}$–BTC, revealing that the partial efficient energy transfer takes place from BTC to doped Eu^{3+} and Tb^{3+} ions, compared with the emission spectra of $Gd_{0.95}Eu_{0.05}$–BTC, $Gd_{0.95}Tb_{0.05}$–BTC and $Y_{0.95}Eu_{0.05}$–BTC, where very weak emission can be observed. Very interestingly, white-light emission can be achieved in the present system, as confirmed by the CIE chromaticity diagram (Fig. 5d).

4. Conclusions

A series of nano/micro-sized lanthanide-based metal–organic frameworks have been developed *via* a simple, rapid, and effective one-step method. 1D nanostructures and 3D assembled nanoarchitectures can be obtained by using different lanthanide ions to chelate benzenetricarboxylic acid. The different forms of splitting are in accordance with the anisotropic crystal structure of Ln–BTC. The as-prepared samples show tunable emission between red and green due to the efficient energy transfer from BTC to doped Eu^{3+} and Tb^{3+} ions. Interestingly, white-light emission from the $Ce_{0.90}Eu_{0.05}Tb_{0.05}$–BTC nano-MOF can be achieved *via* limiting energy transfer. We believe that the present results may serve as a guide for the design and fabrication of novel MOF nanomaterials in a simple way.

Acknowledgements

This work is financially supported by the Natural Science Foundation of Shandong Province (grant no. 20771098) and the Higher Educational Science and Technology Program of Shandong Province, China (grant no. J13LD11).

References

1 (*a*) O. M. Yaghi, M. Obkeeffe, N. W. Ockwig, H. K. Chae, M. Eddaoudi and J. Kim, *Nature*, 2003, **423**, 705; (*b*) X. Zhao, B. Xiao, A. J. Fletcher, K. M. Thomas, D. Bradshaw and M. J. Rosseinsky, *Science*, 2004, **306**, 1012.
2 J. S. Seo, D. Whang, H. Lee, S. I. Jun, J. Oh, Y. J. Jeon and K. Kim, *Nature*, 2000, **404**, 982.
3 O. R. Evans and W. Lin, *Acc. Chem. Res.*, 2002, **35**, 511.
4 (*a*) F. M. Tabellion, S. R. Seidel, A. M. Arif and P. J. Stang, *J. Am. Chem. Soc.*, 2001, **123**, 7740; (*b*) M. E. Kosal, J.-H. Chou, S. R. Wilson and K. S. Suslick, *Nat. Mater.*, 2002, **1**, 118.
5 (*a*) O. Moonhyun and C. A. Mirkin, *Nature*, 2005, **438**, 651; (*b*) Y. M. Jeon, G. S. Armatas, D. Kim, M. G. Kanatzidis and C. A. Mirkin, *Small*, 2009, **5**, 46.
6 K. M. L. Taylor, W. J. Rieter and W. Lin, *J. Am. Chem. Soc.*, 2008, **130**, 14358.
7 Y. H. Wang, B. Li, Y. H. Liu, L. M. Zhang, Q. H. Zuo, L. F. Shi and Z. M. Su, *Chem. Commun.*, 2009, 5868.
8 K. M. L. Taylor, A. Jin and W. Lin, *Angew. Chem., Int. Ed.*, 2008, **47**, 7722.
9 (*a*) H. J. Lee, W. Cho, S. Jung and M. Oh, *Adv. Mater.*, 2009, **21**, 674; (*b*) S. Jung, W. Cho, H. J. Lee and M. Oh, *Angew. Chem., Int. Ed.*, 2009, **48**, 1459.
10 R. C. Huxford-Phillips, S. R. Russell, D. Liu and W. Lin, *RSC Adv.*, 2013, **3**, 14438.
11 K. E. deKrafft, W. S. Boyle, L. M. Burk, O. Z. Zhou and W. Lin, *J. Mater. Chem.*, 2012, **35**, 18065.
12 M. Sindoro, N. Yanai, A. Y. Jee and S. Granick, *Acc. Chem. Res.*, 2014, **47**, 459.
13 J. Della Rocca, D. Liu and W. Lin, *Acc. Chem. Res.*, 2011, **44**, 957.
14 H. Guo, Y. Zhu, S. Qiu, J. A. Lercher and H. Zhang, *Adv. Mater.*, 2010, **22**, 4190.
15 M. Jahan, Q. Bao, J. Yang and K. P. Loh, *J. Am. Chem. Soc.*, 2008, **132**, 14487.
16 (*a*) W. S. Liu, T. Q. Jiao, Y. Z. Li, Q. Z. Liu, M. Y. Tan, H. Wang and L. F. Wang, *J. Am. Chem. Soc.*, 2004, **126**, 2280; (*b*) C. Serre, N. Stock, T. Bein and G. Ferey, *Inorg. Chem.*, 2004, **43**, 3159.
17 (*a*) G. Mancino, A. J. Ferguson, A. Beeby, N. J. Long and T. S. Jones, *J. Am. Chem. Soc.*, 2005, **127**, 524; (*b*) L. D. Carlos, R. A. S. Ferreira, V. Bermudez and S. J. L. Ribeiro, *Adv. Mater.*, 2009, **21**, 509.
18 T. M. Reineke, M. Eddaoudi, M. O'Keeffe and O. M. Yaghi, *Angew. Chem., Int. Ed.*, 1999, **38**, 2590.
19 (*a*) B. L. Chen, Y. Yang, F. Zapata, G. N. Lin, G. D. Qian and E. B. Lobkovsky, *Adv. Mater.*, 2007, **19**, 1693; (*b*) B. L. Chen, L. B. Wang, F. Zapata, G. D. Qian and E. B. Lobkovsky, *J. Am. Chem. Soc.*, 2008, **130**, 6718.
20 (*a*) X. D. Guo, G. S. Zhu, Z. Y. Li, F. X. Sun, Z. H. Yang and S. L. Qiu, *Chem. Commun.*, 2006, 3172; (*b*) X. D. Guo, G. S. Zhu, Z. Y. Li, Y. Chen, X. T. Li and S. L. Qiu, *Inorg. Chem.*, 2006, **45**, 4065; (*c*) Z. Y. Li, G. S. Zhu, X. D. Guo, X. J. Zhao, Z. Jin and S. L. Qiu, *Inorg. Chem.*, 2007, **45**, 5174.
21 Y. Cui, B. Chen and G. Qian, *Coord. Chem. Rev.*, 2014, **273–274**, 76.
22 K. Liu, H. P. You, G. Jia, Y. H. Zheng, Y. H. Song, M. Yang, Y. J. Huang and H. J. Zhang, *Cryst. Growth Des.*, 2009, **9**, 3519.
23 K. Liu, H. P. You, Y. H. Zheng, G. Jia, L. H. Zhang, Y. J. Huang, M. Yang, Y. H. Song and H. J. Zhang, *CrystEngComm*, 2009, **11**, 2622.

24 K. Liu, H. P. You, Y. H. Zheng, G. Jia, Y. Huang, M. Yang, Y. H. Song, L. H. Zhang and H. J. Zhang, *Cryst. Growth Des.*, 2010, **10**, 16.
25 K. Liu, H. P. You, Y. H. Zheng, G. Jia, Y. H. Song, Y. J. Huang, M. Yang, J. J. Jia, N. Guo and H. J. Zhang, *J. Mater. Chem.*, 2010, **32**, 3272.
26 Y. H. Wen, J. K. Cheng, Y. L. Feng, J. Zhang, Z. J. Li and Y. G. Yao, *Chin. J. Struct. Chem.*, 2005, **12**, 1440.
27 (*a*) S. M. Lee, S. N. Cho and J. Cheon, *Adv. Mater.*, 2003, **15**, 441; (*b*) J. P. Liu, Y. Y. Li, X. T. Huang, Z. K. Li, G. Y. Li and H. B. Zeng, *Chem. Mater.*, 2008, **20**, 250; (*c*) W. M. Du, J. Zhu, S. X. Li and X. F. Qian, *Cryst. Growth Des.*, 2008, **8**, 2130.
28 (*a*) L. S. Zhong, J. S. Hu, H. P. Liang, A. M. Cao, W. G. Song and L. J. Wan, *Adv. Mater.*, 2006, **18**, 2426; (*b*) Z. P. Zhang, X. Q. Shao, H. D. Yu, Y. B. Wang and M. Y. Han, *Chem. Mater.*, 2005, **17**, 332.
29 J. Tang and A. P. Alivisatos, *Nano Lett.*, 2006, **6**, 2701.
30 H. Deng, C. M. Liu, S. H. Yang, S. Xiao, Z. K. Zhou and Q. Q. Wang, *Cryst. Growth Des.*, 2008, **8**, 4432.
31 Y. S. Yang, M. L. Gong and Y. Y. Li, *J. Alloys Compd.*, 1994, **207–208**, 112.

